49th AIAA Aerospace Sciences Meeting including the New Horizons Forum and Aerospace Exposition
4 - 7 January 2011, Orlando, Florida

AIAA 2011-1132

Adaptive Wing/Aerofoil Design Optimisation Using MOEA Coupled to Uncertainty Design Method

D. S. Lee[1] and J. Periaux[2]
International Center for Numerical Methods in Engineering (CIMNE)/UPC, Edificio C1, Gran Capitan, s/n.08034 Barcelona Spain.

L. F. Gonzalez[3]
Australian Research Centre Aerospace Automation (ARCAA) School of Engineering System, Queensland University of Technology, Australia.

E. Onate[4]
International Center for Numerical Methods in Engineering (CIMNE)/UPC, Edificio C1, Gran Capitan, s/n.08034 Barcelona Spain.

and

N. Qin[5]
Department of Mechanical Engineering, University of Sheffield, Sir Frederic Mappin Building Mappin Street, Sheffield, S1 3JD, UK

The use of adaptive wing/aerofoil designs is being considered as promising techniques in aeronautic/aerospace since they can reduce aircraft emissions, improve aerodynamic performance of manned or unmanned aircraft. The paper investigates the robust design and optimisation for one type of adaptive techniques; Active Flow Control (AFC) bump at transonic flow conditions on a Natural Laminar Flow (NLF) aerofoil designed to increase aerodynamic efficiency (especially high lift to drag ratio). The concept of using Shock Control Bump (SCB) is to control supersonic flow on the suction/pressure side of NLF aerofoil: RAE 5243 that leads to delaying shock occurrence or weakening its strength. Such AFC technique reduces total drag at transonic speeds due to reduction of wave drag. The location of Boundary Layer Transition (BLT) can influence the position the supersonic shock occurrence. The BLT position is an uncertainty in aerodynamic design due to the many factors, such as surface contamination or surface erosion. The paper studies the SCB shape design optimisation using robust Evolutionary Algorithms (EAs) with uncertainty in BLT positions. The optimisation method is based on a canonical evolution strategy and incorporates the concepts of hierarchical topology, parallel computing and asynchronous evaluation. Two test cases are conducted; the first test assumes the BLT is at 45% of chord from the leading edge and the second test considers robust design optimisation for SCB at the variability of BLT positions and lift coefficient. Numerical result shows that the optimisation method coupled to uncertainty design techniques produces Pareto optimal SCB shapes which have low sensitivity and high aerodynamic performance while having significant total drag reduction.

---

[1] Research Associate, dslee@cimne.upc.edu, ds.chris.lee@gmail.com, AIAA Member.
[2] Profesor, AIAA Associate Fellow.
[3] Lecturer, AIAA Member.
[4] Profesor, AIAA Member.
[5] Profesor, AIAA Associate Fellow.

1
American Institute of Aeronautics and Astronautics

Nomenclature

α	=	angle of attack
BLT	=	boundary layer transition (Note: in aerodynamics, BLT often is used as x_{tr})
Cd_{Total}	=	total coefficient: $Cd_{Total} = Cd_{Viscous} + Cd_{Wave}$
$Cd_{Viscous}$	=	viscous drag coefficient
Cd_{Wave}	=	wave drag coefficient
C_p	=	pressure coefficient
c	=	chord
f	=	fitness functions
K	=	number of uncertainty step size
Re	=	Reynolds number
SCB	=	Shock Control Bump
SCB_H	=	height of SCB (%c)
SCB_L	=	length of SCB (%c)
SCB_P	=	peak position of SCB (%SCB_L)

I. Introduction

IN engineering designs, it is inevitable to face uncertainties design parameters which must be considered in an optimisation task to produce a set of reliable optimal solutions (high performance and low sensitivity). Some of design variables and system input parameters cannot be achieved exactly due to uncertainties in physical quantities such as manufacturing tolerances, material properties, environmental conditions including temperature, pressure, velocity, etc. In conventional design, these parameters are treated as a constant value with assumption. The design model obtained by conventional design methods has good performance at the standard design point, however, using fixed/constant value for uncertain design parameters makes a design model to fluctuate at off-design conditions (high sensitivity: unstable)[1, 2]. An alternative design strategy is the use of robust design under considering uncertainty design parameters to control the sensitivity and performance of the physical model[3, 4]. In this paper, an Robust Active Flow Control (AFC) device design optimisation is conducted.

One of important challenges in aeronautical engineering is to control flow over aerofoil/wing to reduce drag while increasing lift. One of the main reasons is that the drag reduction can save mission operating cost, condense critical aircraft emissions and increase the performance envelope of the aircraft. Such drag reduction can be achieved by implementing a type of AFC called Shock Control Bump (SCB)[5 -8] without the need to design a new aerofoil or wing planform shape.

In this paper, a Natural Laminar Flow aerofoil; RAE 5243 as a baseline design, is investigated with SCB on the suction side to reduce total drag and to extend its critical Mach and lift coefficient at high lift coefficient and transonic flow speeds. Two optimisation test cases are conducted using advanced Evolutionary Algorithms (EAs)[9]; the first test considers Boundary Layer Transition (BLT) position at 45% of chord. The second test is conducted at the variability of BLT positions and lift coefficient using robust/uncertainty design technique. In conventional design, aerofoil optimisation is conducted at fixed/constant BLT position. However, BLT cannot be assumed as a constant value in real design problem especially for the AFC device design since the shape of AFC device will change the position of BLT. Therefore the BLT location is considered as one of uncertainty design parameters.

The paper will show how to control the design quality under considering uncertain design parameters and also demonstrate how to control the transonic flow on current aerofoil using a SCB.

The rest of paper is organised as follows; Section II describes optimisation method and uncertainty design techniques. Aerodynamic analysis tools are described in Section III. Section IV demonstrates the use of SCB. Section V considers SCB shape design optimisation using single-objective and robust design approach considering uncertain BLT positions. The paper concludes with a summary and some future research avenues in Section VI.

II. Robust/Uncertainty Design Methods

The method couples a Hierarchical Asynchronous Parallel Multi-Objective Evolutionary Algorithms (HAPMOEA) with an algorithm for SCB geometry, a module for robust design and several aerodynamic analysis tools[9]. The algorithm is based on Evolution Strategies[10] and incorporates with the concepts of Covariance Matrix Adaptation (CMA), Distance Dependent Mutation (DDM), a hierarchical topology, asynchronous evaluation[11 -15]

and a Pareto tournament selection that is applicable to single or multi-objective problems[1, 2]. The hierarchical topology can provide different models including precise, intermediate and approximate models. Each node belonging to the different hierarchical layer can be handled by a different EAs code. HAPMOEA has also been coupled to uncertainty design techniques as shown in References 1, 2, 4. Details and validation of HAPMOEA can be found in Reference 9.

A. Robust/Uncertainty Design

A Robust Design method, also called the Taguchi Method (uncertainty), pioneered by G. Taguchi[3] in 1978, improves the quality of engineering productivity. An optimisation problem can be defined as;

$$\text{maximisation or minimisation } f = f\left(x_1,...,x_n,x_{n+1},...,x_m\right)$$

where $x_1,...,x_n$ represent design parameters and $x_{n+1},...,x_m$ represent uncertainty parameters. The range of uncertainty design parameters can be defined by using two statistical functions; mean ($\bar{x}$) and variance ($\delta x = (\sigma x)^2$) as part of the Probability Density Function (PDF).

The Taguchi optimization method minimises the variability of the performance under uncertain design conditions. Therefore in order to perform an optimisation with uncertainties, the fitness function(s) should be associated with two statistical formulas; the mean value $\bar{f}$ and its variance δf or standard deviation $\sigma f = \sqrt{\delta f}$.

$$\bar{f} = \frac{1}{K}\sum_{i=1}^{K} f_i \tag{1}$$

$$\delta f = \frac{1}{K-1}\left(\sum_{i=1}^{K}\left(f_i - \bar{f}\right)^2\right) \tag{2}$$

where K denotes the number of subintervals of variation flow conditions.

The values obtained by the mean ($\bar{f}$) and the variance (σf) or standard deviation (δf) represent the reliability of model in terms of the magnitude of performance and stability/sensitivity at a set of uncertain design conditions.

B. Robust Design Method Implementation for Single-Objective Design Optimisation Problems

The problem definition can be written with the fitness functions associated with a mean (Eq. (1)) and variance/standard deviation (Eq. (2)) as an uncertainty based multi-objective design problem if a single-objective aerofoil design optimisation problem considers a minimisation of drag ($f = \min(C_D)$) at a single flight condition (M_S). The robust design fitness functions are shown in Eq. (3) and Eq. (4) while a single flight condition becomes a set uncertainty flight conditions; $M_{\infty_K} \in \left[M_S - \varepsilon, M_S, M_S + \varepsilon\right]$ or $\overline{M_\infty}$ and σM_∞ .

$$\overline{C_D} = \frac{1}{K}\sum_{i=1}^{K} C_{Di} \tag{3}$$

$$\sigma C_D = \sqrt{\delta C_D} = \sqrt{\frac{1}{K-1}\left(\sum_{i=1}^{K}\left(C_{D_i} - \overline{C_D}\right)^2\right)} \tag{4}$$

where K represents the number of uncertainty conditions.

Consequently, the major role of uncertainty technique is to improve C_D quality with low drag coefficient and drag sensitivity at uncertain flight conditions by computing mean and variance of criteria.

III.   Aerodynamic Analysis Tools

In this paper, the Euler + Boundary layer solver: MSES written by Drela[17] is utilised. The MSES software is a coupled viscous/inviscid Euler method for the analysis and design of multi-element/single-element airfoils. It is a based on a streamline-based Euler discretization and a two-equation integral boundary layer formulation which are coupled through the displacement thickness and solved simultaneously by a full Newton method. To obtain a prescribed lift coefficient C_l, the angle of attack α of the aerofoil is adapted. Details of MSES can be found in Reference 17 and the validation of MSES compared to the wind tunnel data can be found in Reference 18.

IV.   Wave Drag Reduction via. Active Flow Control Bump

At transonic speed, the flow over the high camber wing causes shock waves where there is a large changes of gas properties and the flow becomes irreversible. Through the shock, total pressure decreases and entropy increases which means an increase in the wave drag. Ashill et al. 1992 [5] proposed the concept of a transonic bump which so-called Shock Control Bump (SCB) by using geometry adaption on an aerofoil. As illustrated in Figure 1, the most common design variables for the SCB are: length (SCB_L), height (SCB_H) and peak position (SCB_P) and, the center of SCB (i.e. 50% of SCB_L) is located where the shock occurs on the transonic aerofoil design.
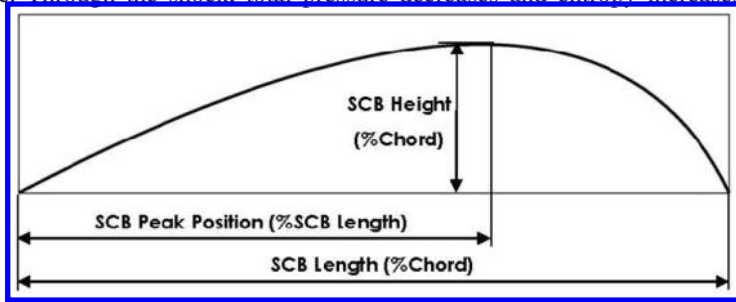
Figure 1. Design Components of Shock Control Bump.

Figure 2 illustrates the concept and benefit of using SCB. The transonic flow over normal aerofoil without SCB accelerates to supersonic and the pressure forms a strong shock that leads a high Cd_{wave} however the pressure difference over the SCB causes the supersonic flow to decelerate to subsonic Mach numbers by a weaker shock wave which leads to lower wave drag.
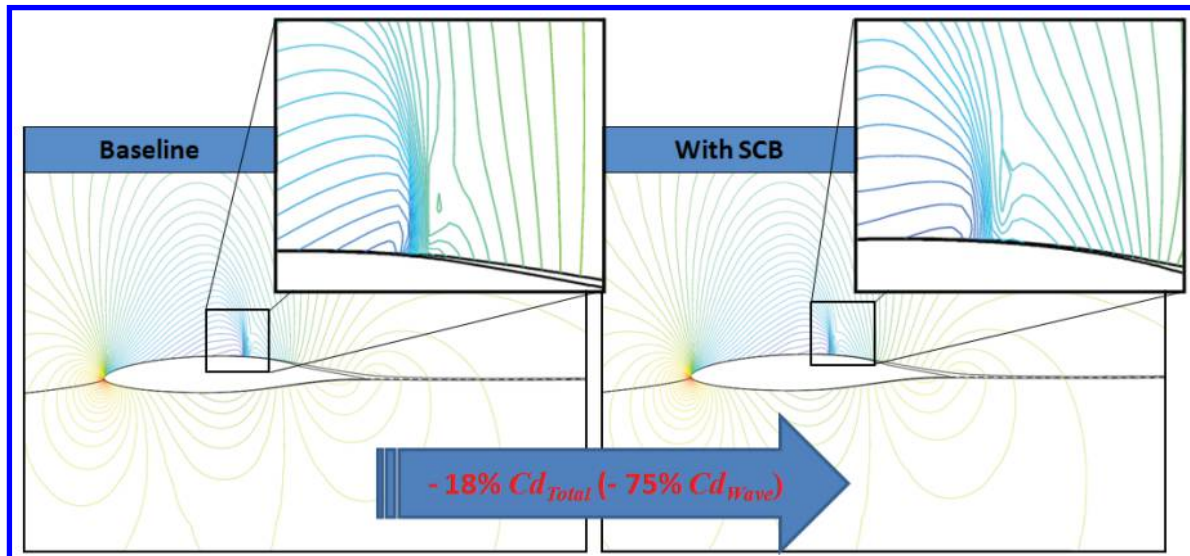
Figure 2. Comparison of aerofoil without (left) and with SCB (right).

V.   Active Flow Control Bump (SCB) Design Optimisation

The natural laminar flow aerofoil; RAE 5243 [6] is selected as a baseline design. The aerofoil has a maximum thickness of 0.14 at 41%c from the leading edge and a maximum camber of 0.0186 at 54.0%c. The baseline design is tested at flow conditions $M_\infty = 0.68$, $C_l = 0.82$, $Re = 19.0 \times 10^6$ with a Boundary Layer Transition (BLT) at 45%

American Institute of Aeronautics and Astronautics

of chord from the leading edge. Figure 3 shows the *Cp* contours obtained by MSES. It can be seen that there is a strong normal shock on the suction side of baseline design at 45%c BLT conditions.

The shock occurs at 59.5% of chord where a BLT position at 45%c. This baseline design will be compared to the optimal SCB designed to minimise the total drag (Cd_{Total}) in Section V.A: Single-objective design optimisation and Section V.B: Robust multiobjective design.
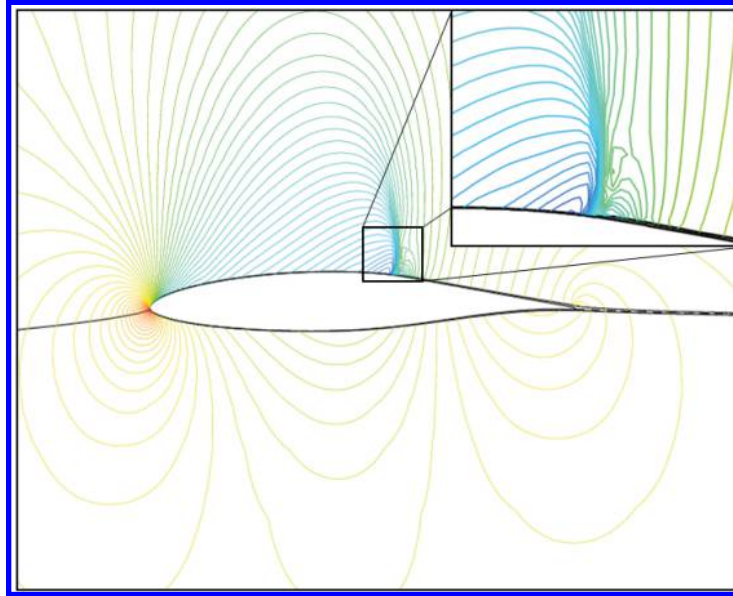
Figure 3. *Cp* contour obtained by RAE 5243.

A. SCB Shape Design Optimisation with Boundary Layer Transition position at 45%c
Problem Definition

This test case considers a single objective SCB design optimisation on the upper surface of the RAE 5243 aerofoil to minimise the total drag at flow conditions $M_\infty = 0.68$, $C_l = 0.82$, Re = 19.0×10^6 with a BLT at 45%c from the leading edge. The fitness function is shown in Eq. (5).

$$fitness\left(f \right) = \min\left(Cd_{Total} \right) = \min\left(Cd_{Viscous} + Cd_{Wave} \right) \tag{5}$$

Design Variables

The design variable bounds for the SCB geometry are illustrated in Table 1. The centre of the SCB (50% of SCB length) will be located at the shock where the flow speed transits from supersonic to subsonic (60% of chord in this case). The SCB spans from approximately 45%c to 75%c if the SCB length is 30%c.

Table 1. SCB design variables and bounds.

Design Variables	Lower bound	Upper bound
SCB_L	0	30
SCB_H	0	5
SCB_P	0	100

Note: Peak position is in % of SCB length (SCB_L).

The maximum length of SCB is limited to 30%c to prevent the SCB over flap and aileron control surfaces which are usually located from 75%c to trailing edge (100%c).

Implementation

The optimisation was computed using HAPMOEA coupled to MSES using a single 4×2.8 GHz processor with the following details on multi-resolution/population hierarchical populations [7].

American Institute of Aeronautics and Astronautics

- 1st Layer: Population size of 10 with a computational grid of 36×213 points (Node0).
- 2nd Layer: Population size of 20 with a computational grid of 24×131 points (Node1, Node2).
- 3rd Layer: Population size of 30 with a computational grid of 36×111 points (Node3 ~ Node6).
Note: The difference in accuracy between the first and the third layers is less than 5%.

Numerical Results
The algorithm was allowed to run for 24 hours (as time stopping criterion) and for 6,135 function evaluations. Convergence occurred after 1,826 function evaluations (seven and half hours) as shown in Figure 4.
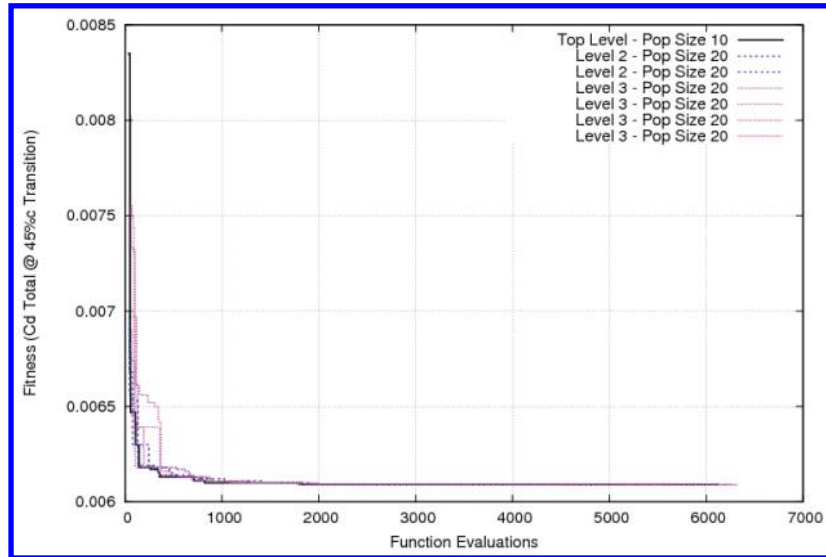
Figure 4. Convergence objective for SCB design at 45%c BLT.

Table 2 compares the aerodynamic characteristics obtained by the baseline design (RAE 5243) and the baseline design with the optimal SCB. It can be seen that applying SCB on upper surface of RAE 5243 aerofoil reduces the wave drag by 95% which leads to 40% total drag reduction. This optimal SCB improves *L/D* by 65%.

Table 2. Aerodynamic characteristics obtained by single-objective design approach.

Aerofoil	Cd_{Total}	Cd_{Wave}	L/D
Baseline (RAE 5243)	0.01003	0.0032	81.72
with optimal SCB	0.00609 (- 40%)	0.00014 (- 95%)	134.56 (+ 65%)

Note: C_l is fixed to 0.82.

The design variables for the optimal SCB are shown in Table 3. Figure 5 compares the geometry of the baseline design and baseline with optimal SCB. The baseline (RAE 5243) design with optimal SCB has a maximum thickness of 0.14 ($t/c_{max} = 0.14$) at 41%c from the leading edge and the maximum camber is 0.0215 at 63.1%c. Adding the optimal SCB increases the maximum camber by 0.003, and the camber position moves towards to the trailing edge by 9%c while keeping the same maximum thickness as the baseline design.

Table 3. Optimal SCB design components.

Variables	SCB_L (%c)	SCB_H (%c)	SCB_P (%SCB_L)
SCB	29.22	1.04	67.7

Note: Peak position (SCB_P) is in % of SCB length. The optimal SCB is located between $x = 0.4516$, $y = 0.0858$ and $x = 0.7440$, $y = 0.0475$.

American Institute of Aeronautics and Astronautics
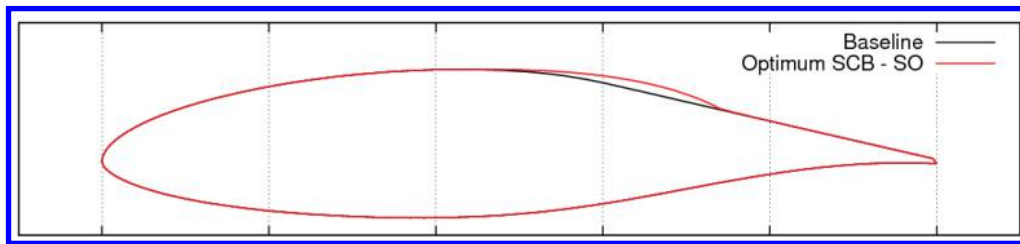
Figure 5. Baseline design with the optimal SCB at 45%c BLT.

Figures 6 a) and 6 b) show the Cp contour and distribution obtained by the baseline design with optimal SCB. It can be seen that the strong shock on the baseline design shown in Figure 3 is now 95% weaker by adding SCB. In addition, the sonic point where Mach is 1.0 is moved towards to the trailing edge by 7.0%c.
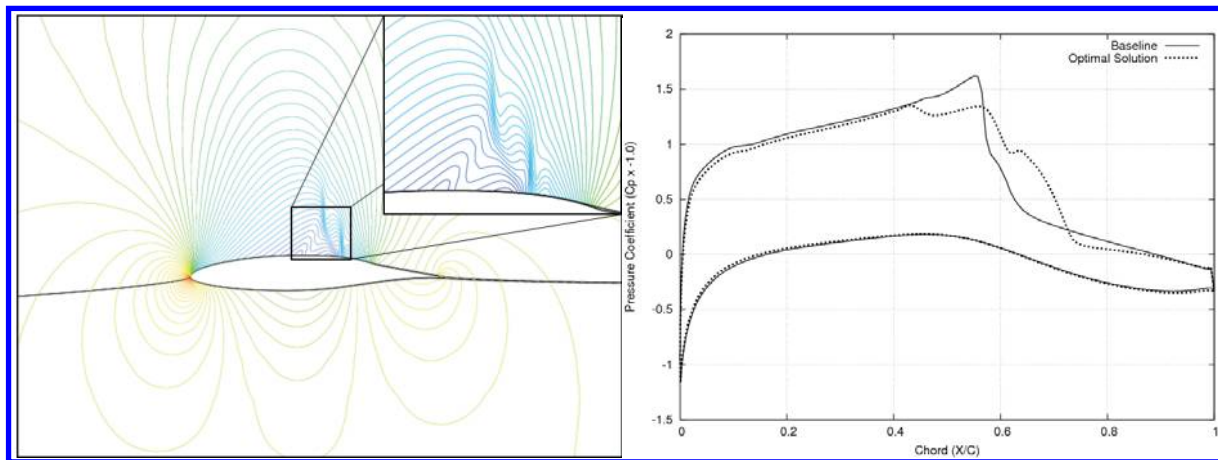
Figure 6. Cp contour a), Cp distribution b) obtained by RAE 5243 with the optimal SCB at 45%c BLT.

Figures 7 a) and 7 b) compare total drag (Cd_{Total}) and wave drag (Cd_{Wave}) distributions obtained by the baseline design and one with the optimal SCB along the Mach range i.e. $M_\infty \in [0.5:0.75]$ with $Cl_{Fixed} = 0.82$, Re $= 19.0 \times 10^6$ with a BLT at 45%c. The baseline design with SCB starts to produce lower total drag when Mach number is higher than 0.67. By adding the optimal SCB, the baseline design reduces its total drag by 40% and its wave drag by 95% at the standard flight condition marked with dashed line. The critical Mach number for baseline design ($M_C = 0.64$) is extended to 0.68 due to the optimal SCB.
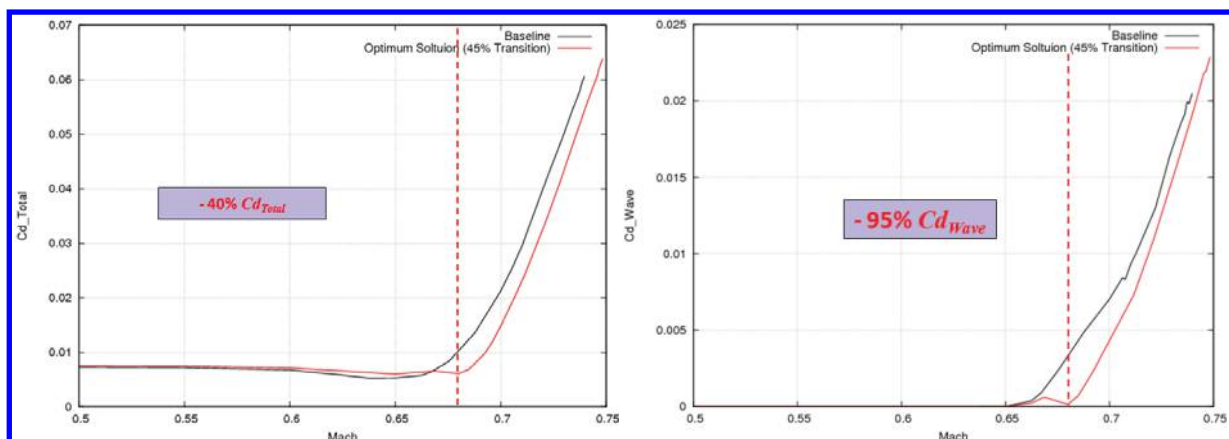
Figure 7. Cd_{Total} (a) & Cd_{Wave} (b) vs. Mach at 45%c BLT.

Figures 8 a) and 8 b) compare total drag distributions obtained by the baseline design and one with the optimal SCB for a C_l range i.e. $C_l \in [0.1:1.1]$ with $M_\infty = 0.68$, Re $= 19.0 \times 10^6$ with a BLT at 45%c. The baseline design

7

American Institute of Aeronautics and Astronautics

with SCB starts to produce lower total drag when C_l number is higher than 0.65. The critical C_l number for the baseline design ($C_{lc} = 0.25$) is extended to 0.79 by applying optimal SCB on the suction side of baseline design.
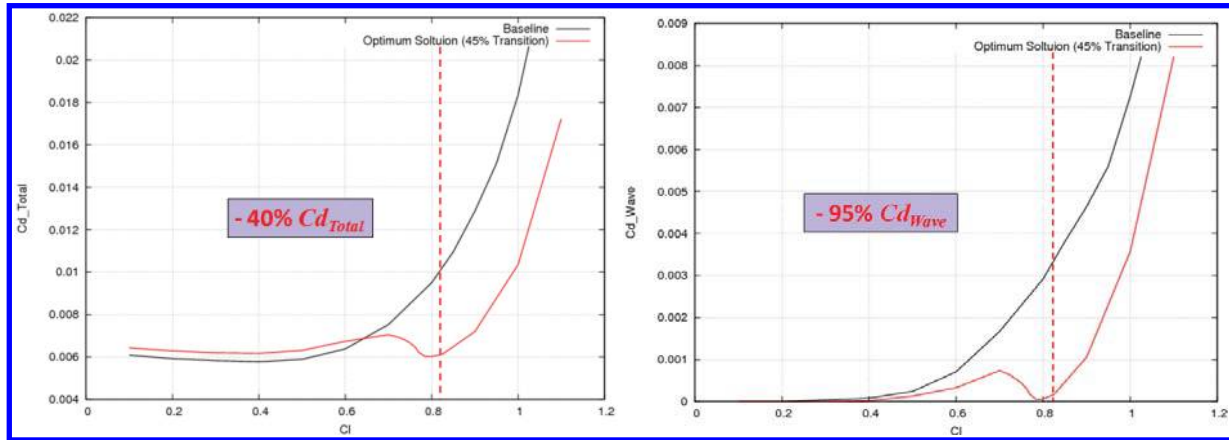
Figure 8. Cd_{Total} **(a) &** Cd_{Wave} **(b) vs.** *Cl* **at 45%c BLT.**

Even though good results were obtained by using the single-objective design approach, the optimal SCB produces an irregular/undesirable Cd_{Total} fluctuation at a range of C_l from 0.6 to 0.82 (shown in Figures 8 a) and 8 b)). This optimal solution is an over-optimised solution which does not perform well before reaching the standard flow/flight conditions. This fluctuation should be treated as uncertainty in the design parameters and the design engineer should take into account during the optimization. Therefore, it is necessary to use an uncertainty design technique to produce a set of solutions which have both low mean and sensitivity (no fluctuation: stable) Cd_{Total} by considering variable C_l values and BLT positions.

B. Robust SCB Shape Design Optimisation with Uncertainty in Boundary Layer Transitions location
Problem Definition

This test case considers a robust multi-objective SCB design optimisation on the upper surface of the RAE 5243 aerofoil to minimize mean and standard deviation of total drag ($\overline{Cd_{Total}}$, σCd_{Total}) at flow conditions $M_\infty = 0.68$ and Re = 19.0×10^6. In addition, two C_l and three Boundary Layer Transition (BLT) positions are considered i.e. C_l = [0.7, 0.82], *BLT* = [25%c, 37.5%c, 50%c] for uncertainty design parameters. These can be statistically rewritten as $\overline{BLT}$ = 37.5%c, σBLT = 12.5%c. The candidate SCB model will be evaluated at six flight conditions (3 BLT × 2 C_l) as shown in Table 4. The fitness functions are shown in Eq. (6) and Eq. (7) respectively.

$$f_1 = \min\left(\overline{Cd_{Total}}\right) = \frac{1}{n \times m} \sum_{i=1}^{n} \sum_{j=1}^{m} Cd_{Total_{ij}} \tag{6}$$

$$f_2 = \min\left(\sigma Cd_{Total}\right) = \sqrt{\frac{1}{n \times m - 1} \sum_{i=1}^{n} \sum_{j=1}^{m} \left(Cd_{Total_{ij}} - \overline{Cd_{Total}}\right)^2} \tag{7}$$

where *n* and *m* represent the number of boundary layer transition positions and C_l conditions.

Table 4.   Variability of Flight Conditions (3 BLT positions × 2 C_l).

Variability	Flight condition1	Flight condition2	Flight condition3	Flight condition4	Flight condition5	Flight condition6
BLT position	25.0%c	25.0%c	37.5%c	37.5%c	50.0%c	50.0%c
C_l	0.7	0.82	0.7	0.82	0.7	0.82

Design Variables

8
American Institute of Aeronautics and Astronautics

The design variable bounds for the SCB geometry were illustrated in Table 1. The centre of the SCB (50% of SCB_L) will be located at the sonic point where the flow speed transits from supersonic to subsonic (58% of chord) at 37.5%c BLT. The SCB will be located between 43%c and 73%c if SCB length is assigned as 30%c.

Implementation

The optimisation was computed using HAPMOEA coupled to MSES at the following details on multi-resolution/population hierarchical populations [7].

- 1st Layer: Population size of 15 with a computational grid of 36×213 points (Node0).
- 2nd Layer: Population size of 20 with a computational grid of 24×131 points (Node1, Node2).
- 3rd Layer: Population size of 40 with a computational grid of 36×111 points (Node3 ~ Node6).

Note: The difference in accuracy between the first and third layers is less than 5%.

Numerical Results

The algorithm was allowed to run for 50 hours and 2,450 function evaluations using a single 4×2.8 GHz processor. Pareto optimal solutions are shown in Figure 9 and their sensitivity and performance are compared to the baseline design and the optimal design from single-objective approach (Section V.A). It can be seen that all Pareto member dominate the baseline for the second fitness function (standard deviation of Cd_{Total}: σCd_{Total}) while Pareto members 1 to 9 dominate the baseline design in terms of mean and standard deviation of Cd_{Total}. Pareto members 1 to 3 dominate the optimal design from Section V.A. Pareto members 1 and 4 are selected to compare aerodynamic performance to the baseline design and optimal solution from Section V.A.
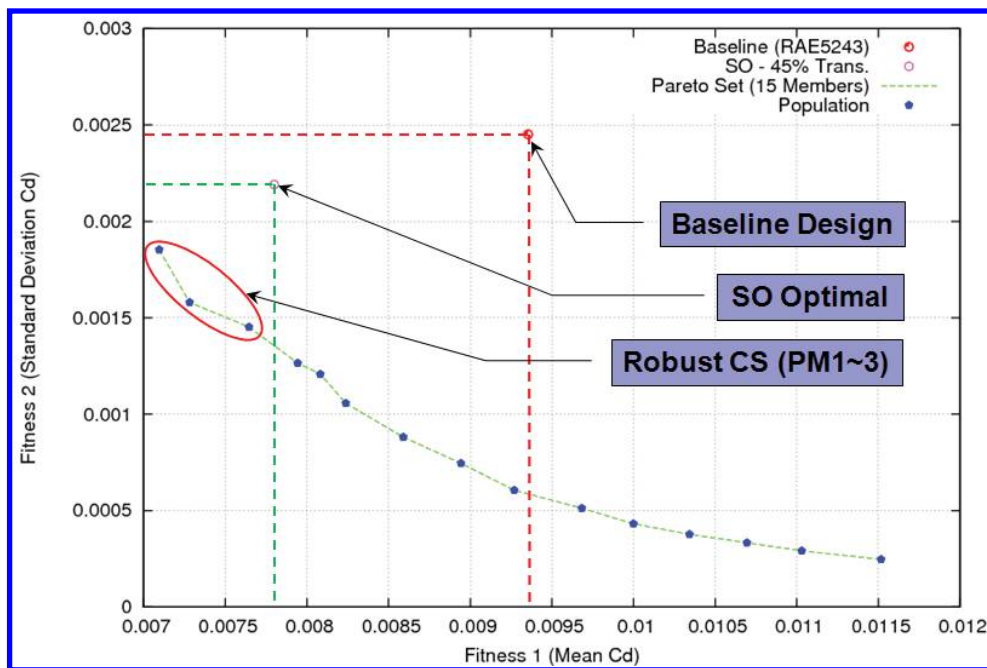
Figure 9. Pareto optimal front for robust SCB design at the variability BLT (BLT = 37.5%c, σBLT = 12.5%c and C_l = [0.7, 0.82]) (Note: SO and CS represent the single-objective approach and compromised solutions respectively.

Table 5 compares the aerodynamic characteristics obtained by the baseline design (RAE 5243) and the baseline design with SCB obtained by Pareto members 1 to 4. It can be seen that applying the optimal SCB obtained by Pareto member 1 on the suction side of RAE 5243 aerofoil reduces the mean total drag by 24%. This optimal SCB improves *L/D* by 32.0%.

Table 5. Comparison of fitness value obtained by robust design approach considering six uncertainty conditions.

Aerofoil	$\overline{Cd_{Total}}$	σCd_{Total}	$\overline{L/D}$
Baseline	0.00935	0.00245	87.70
Optimal solution (Section V.A)	0.00780 (- 17%)	0.00219 (- 11%)	105.13 (+ 20%)
with Pareto Member 1 - SCB	*0.00709 (- 24%)*	*0.00185 (- 24%)*	*115.66 (+ 32%)*
with Pareto Member 2 - SCB	0.00728 (- 22%)	0.00158 (- 35%)	112.64 (+ 28%)
with Pareto Member 3 - SCB	0.00764 (- 18%)	0.00145 (- 41%)	107.33 (+ 22%)

Note: PM$_i$ represents Pareto optimal member obtained by robust design optimisation.

The mean and standard deviations obtained by the baseline design, single-objective and robust Pareto members can be compared using Cumulative Distribution Function (CDF) and Probability Density Function (PDF). Figure 10 a) shows the CDF obtained by the baseline design, the optimal from single-objective (marked as SO optimal in Figure 10) and the robust compromise Pareto solutions (marked as Robust CS). It can be seen that all solution obtained by single-objective and robust design methods have lower mean total drag when compared to the baseline design. Pareto member 1 reduces the mean total drag by 24% when compared to the baseline while the optimal obtained by the single-objective approach reduces total drag by 17%. The standard deviation (sensitivity) can be represented by evaluating gradient of the lines to the CDF value of 0.5 or 1 (steep gradient = low sensitivity). The PDF is plotted in Figure 10 b) to have a clear sensitivity comparison between the baseline design, single-objective, robust design method. It can be seen that all solution obtained by the single-objective and robust design methods have lower sensitivity (narrower and taller bell curve). Pareto member 3 obtained by the robust design method has 41% total drag sensitivity reduction when compared to the baseline design while the optimal obtained by single-objective approach reduces total drag by only 11%. In other words, the robust design method has capabilities to produce a set of solutions which have better performance and sensitivity when compared to the single-objective optimisation method.
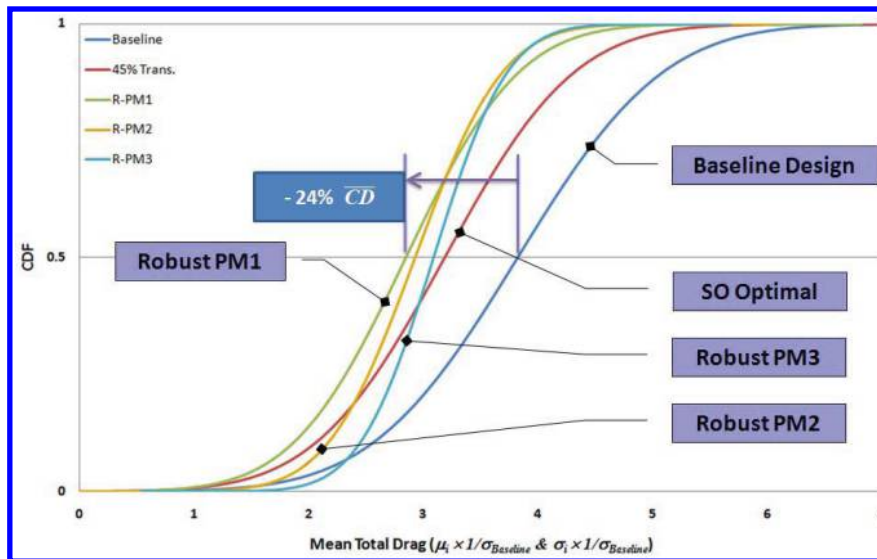
Figure 10 a). Todal mean drag comparison using CDF.
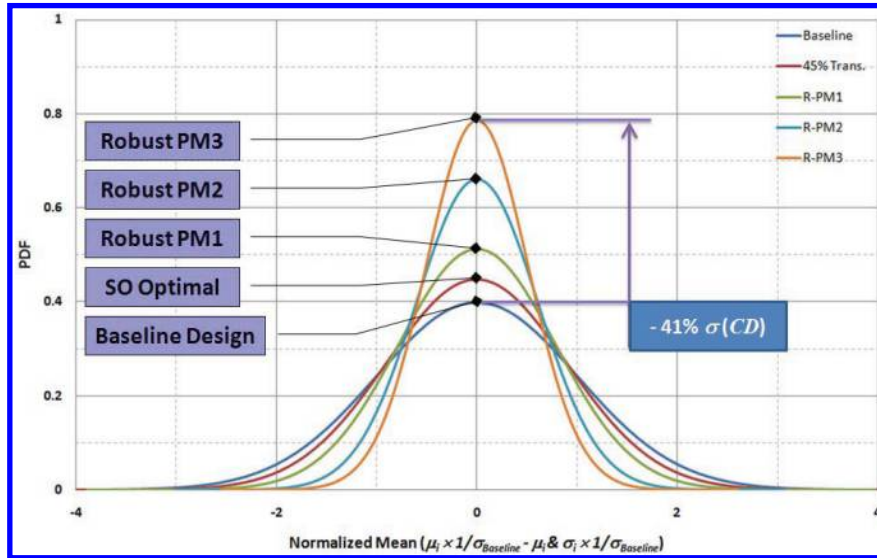
Figure 10 b). Standard deviation (Sensitivity) of total drag comparison using PDF.

For the detailed sensitivity analysis, the baseline design, the optimal solution obtained in Section V.A and Pareto members 1 to 3 are selected and their $\overline{Cd_{Total}}$ (Eq. 7) and σCd_{Total} (Eq. 8) are recomputed at the variability of $\overline{BLT}$ = 37.49%c, σBLT = 0.0729%c [25.0%c:50.0%c] and the variability of $\overline{Cl}$ = 0.761, σCl = 0.0385, [0.7:0.82]. In total, five hundred non-uniformly distributed flight conditions (50 BLT positions × 10 C_l) obtained by Latin Hypercube Sampling [19] are considered. Table 6 compares the aerodynamic characteristics obtained by the baseline design and the optimal solution obtained in Section V.A and Pareto members 1 -3. It can be seen that the both optimal solutions produce lower total mean drag and drag sensitivity respect to five hundred uncertain design conditions (boundary layer transition location and lift coefficient). Applying the optimal SCB obtained by Pareto member 1 produces 26% lower total drag while lowering the drag sensitivity by 22% when compared to the baseline design. The sensitivity obtained by the baseline design and all solutions is more than two and half times lower due to increment of the number of uncertainty design conditions from six to five hundred. In addition, Figure 11 compares mean and standard deviation using CDF and PDF.

One thing can be noticed is that $\overline{Cd_{Total}}$ and σCd_{Total} behaviors obtained by CDF and PDF (shown in Figure 10) considering six uncertain flight conditions are similiar to $\overline{Cd_{Total}}$ and σCd_{Total} obtained by CDF and PDF (shown in Figure 11) considering five hundred flight conditions between the baseline design and Pareto members 1 to 3. In other words, the simplified robust method with six uncertain flight conditions still produces both lower total mean drag and drag sensitivity respect to the variability of boundary layer transition positions and lift coefficient.

Table 6. Comparison of mean and standard deviation of drag obtained by the baseline design, single optimal solution and the Pareto members under considering five hundred uncertainty conditions.

Aerofoil	$\overline{Cd_{Total}}$	σCd_{Total}	$\overline{L/D}$
Baseline	0. 00919	0.000893	83.31
Optimal solution (Section V.A)	0.00705 (- 23%)	0.000756 (- 15%)	109.59 (+ 31%)
with Pareto Member 1 - SCB	*0.00678 (- 26%)*	*0.000696 (- 22%)*	*113.17 (+ 36%)*
with Pareto Member 2 - SCB	0.00720 (- 22%)	0.000591 (- 34%)	106.38 (+ 28%)
with Pareto Member 3 - SCB	0.00757 (- 18%)	0.000498 (- 44%)	100.93 (+ 21%)
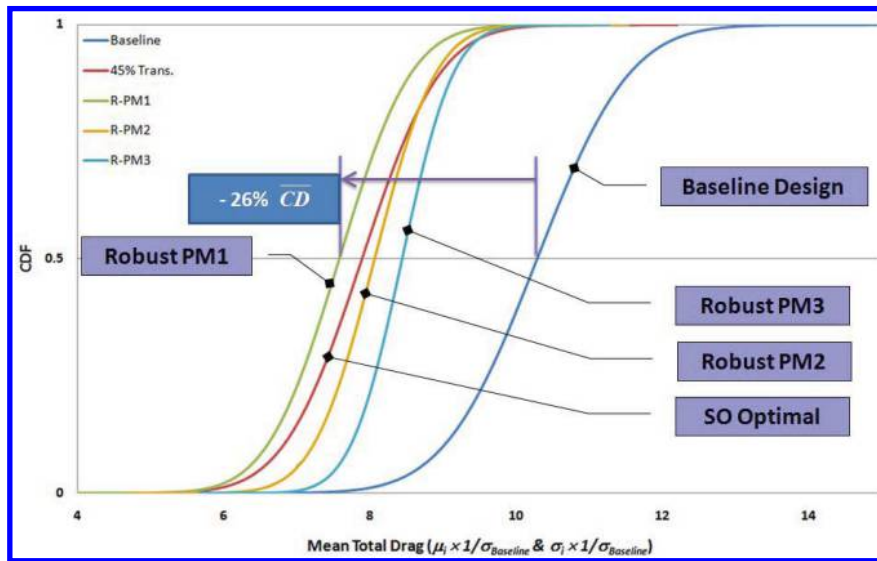
Figure 11 a). Total mean drag comparison using CDF with five hundred uncertainty flight conditions.
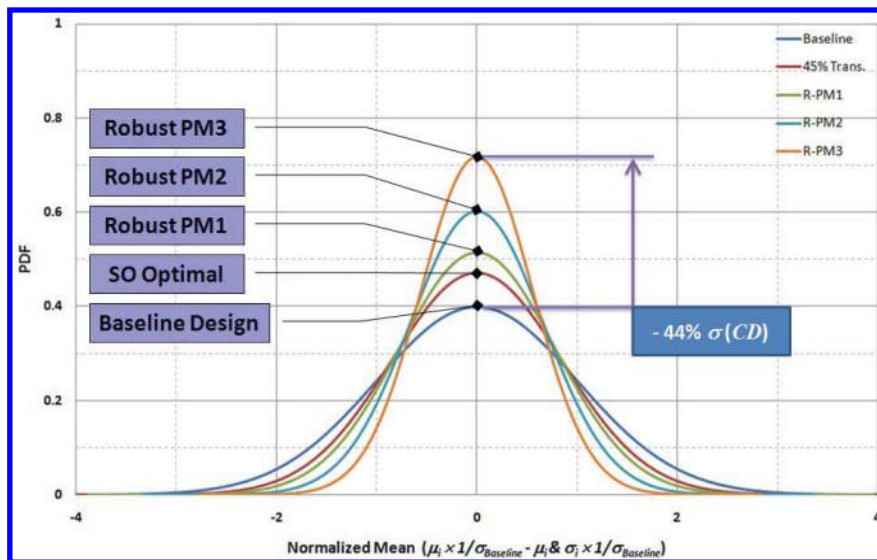
Figure 11 b). Standard deviation (Sensitivity) of total drag comparison using PDF with five hundred uncertainty flight conditions.

The design parameters of the SCB obtained by Pareto members 1 -3 are shown in Table 7. It can be seen that the length and height of SCB are reduced by approximately 5%c and 0.4%c respectively when compared to the optimal solution from Section V.A (Table 3). Figure 12 compares the geometry of the baseline design and baseline with optimal SCBs. The baseline (RAE 5243) design with SCB obtained by Pareto member 1 has a maximum thickness 0.14 ($t/c_{max} = 0.14$) at 41%c from the leading edge while a maximum camber 0.0205 at 62.5%c. Adding the SCB obtained by Pareto member 1 increases the maximum camber by 0.002 and its position is moved towards to the trailing edge by 8.5%c while keeping the same maximum thickness as the baseline design.

Table 7. Pareto optimal SCB design components.

Variables	SCB_L (%c)	SCB_H (%c)	SCB_P (%SCB_L)
Pareto Member 1 - SCB	25.93	0.76	69.3
Pareto Member 2 - SCB	27.12	0.85	76.2
Pareto Member 3 - SCB	26.45	0.75	81.3

Note: Peak position is in % of SCB length. The Pareto Member 1-SCB is located between ($x = 0.4490, y = 0.0859$) and ($x = 0.7083, y = 0.0540$).
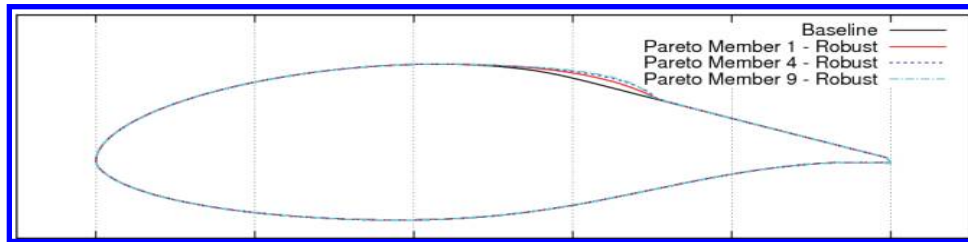
Figure 12. Baseline design with the optimal SCB at 45%c BLT.

Figures 13 a) and 13 b) show the pressure contour and distribution obtained by the baseline design and Pareto member 1 at 45%c boundary layer transition position. It can be seen that the strong shock on the baseline design shown in Figure 3 is 77% weaker by adding SCB on the suction side. The SCB for Pareto member 1 reduces the total drag by 35% and improves the lift to drag ratio by 53%. In addition, the sonic point where Mach is 1.0 is moved towards to the trailing edge by 2.0%c.
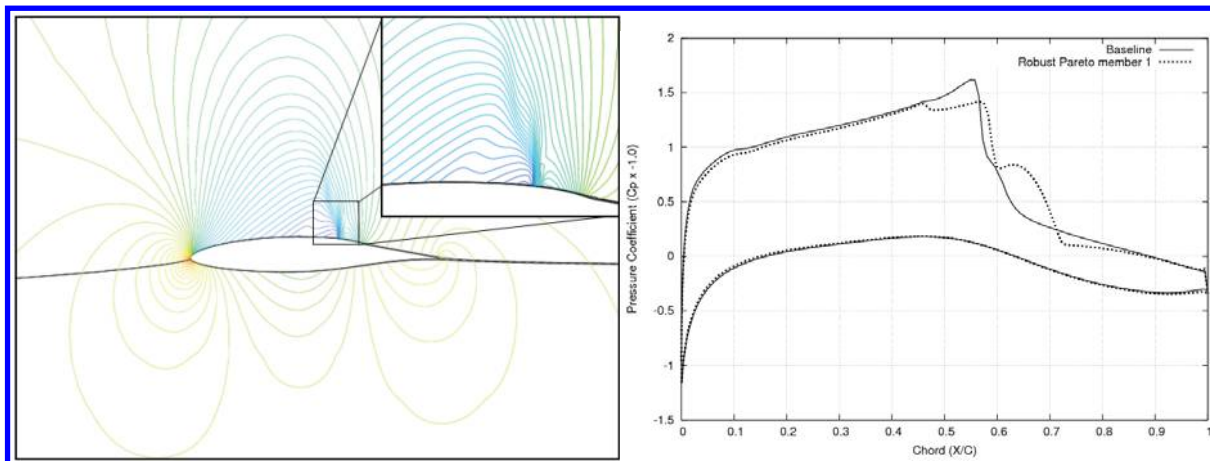
Figure 13. *Cp* contour a), *Cp* distributions b) obtained by RAE 5243 with the PM1-SCB at 45%c BLT.

Figure 14 a) compares the total drag (Cd_{Total}) distributions obtained by the baseline design, the optimal solution obtained in Section V.A and Pareto members 1 and 4. The flight conditions are; $M_\infty \in [0.6:0.72]$ with $Cl_{Fixed} = 0.82$, Re = 19.0×10^6 and the boundary layer transition at 45%c. It can be seen that all solution obtained by single-objective and robust design method have lower total drag when the Mach number is higher than 0.67. The optimal solution from Section V.A produces lower total drag (- 40%) at Mach number 0.68 and Pareto members 1 and 4 reduce the total drag by 35% and 27% respectively. Pareto member 1 has lower drag compared to other solutions when Mach is lower than 0.6775 while Pareto member 4 produces lower drag when Mach is higher than 0.685.
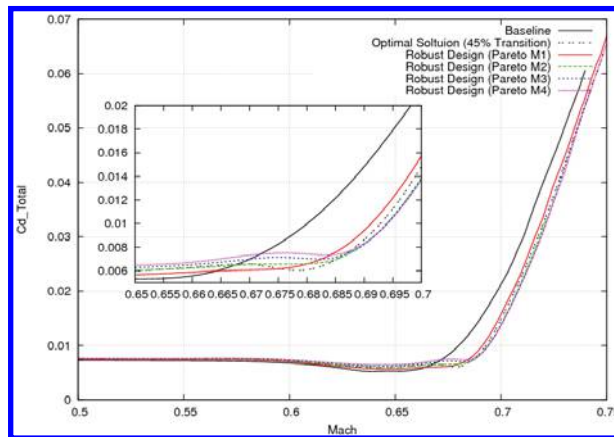
Figure 14 a). Cd_{Total} **vs. Mach at 45%c BLT.**

Figure 14 b) compares total drag (Cd_{Total}) distributions at the flow conditions; $C_l \in [0.1:1.1]$ with $M_{Fixed} = 0.68$, Re $= 19.0 \times 10^6$ and the boundary layer transition at 45%c. Even though the optimal solution obtained by single-objective method produces lower total drag, Pareto members 1 -4 have a stable total drag distribution at C_l range [0.6:0.82] without fluctuation due to the stable wave drag. Figure 14 c) compares wave drag (Cd_{Wave}) distributions obtained by the baseline design, single-objective and robust design methods. It can be seen that Pareto members 1 -4 produce stable wave drag when compared to the baseline design and the single-objective approach.

One thing should be noticed is that the critical lift coefficient numbers (Cl_C) for the baseline design, the optimal solution obtained by the single-objective and Pareto members obtained by the robust design method are 0.3, 0.4 and 0.5 respectively.
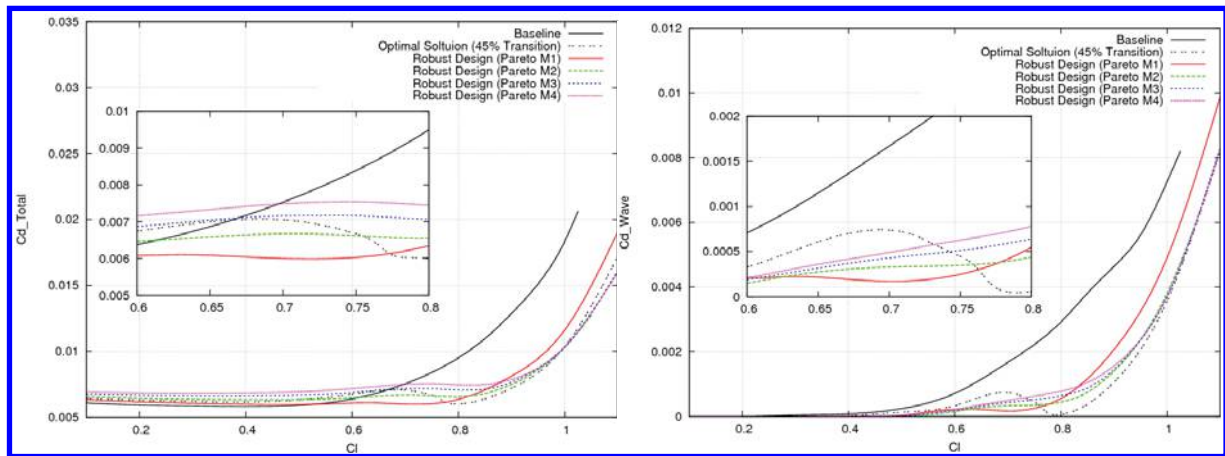
Figure 14. Cd_{Total} **(b) &** Cd_{Wave} **(c) vs.** Cl **at 45%c BLT.**

Figure 15 a) compares the total drag distributions at a range of Mach numbers i.e. $M_{\infty} \in [0.5:0.75]$ with $Cl_{Fixed} = 0.82$, Re $= 19.0 \times 10^6$ and the boundary layer transition at 25%c. The optimal solution obtained in Section V.A, and Pareto members 1 -4 produce lower total drag compared to the baseline design when the Mach number is higher than 0.665. The optimal solution (Section V.A), Pareto members 1 and 4 reduce the total drag by 25%, 24% and 23% respectively when compared to the baseline design. Pareto member 1 has lower drag when Mach is lower than 0.6775 while Pareto member 4 has lower drag when Mach is lower than 0.685.

14
American Institute of Aeronautics and Astronautics
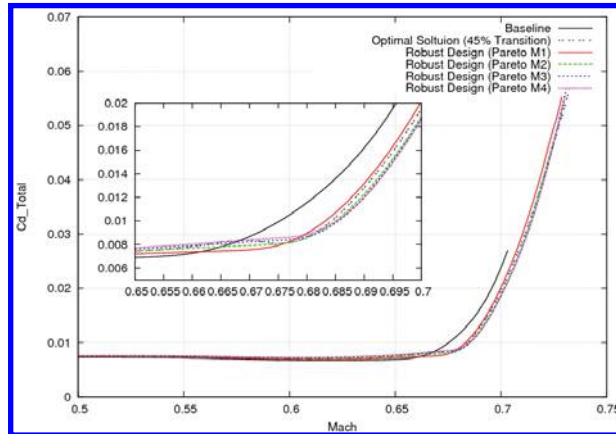
Figure 15 a). Cd_{Total} **vs. Mach at 25%c BLT.**

Figure 15 b) compares total drag distributions at a range of C_l i.e. $C_l \in [0.1:1.1]$ with $M_{Fixed} = 0.68$, Re = 19.0×10^6 and the boundary layer transition at 25%c. The optimal solution from Section V.A fluctuates at the range of $C_l = [0.6: 0.82]$ while Pareto members 1 and 4 have a stable C_l distribution. Figure 15 c) compares wave drag (Cd_{Wave}) distributions obtained by the baseline design, single-objective and robust design methods. It can be clearly seen that Pareto members 1 -4 produce stable wave drag when compared to the baseline design and single-objective approach. It should be noticed that the critical lift coefficient numbers (Cl_C) for the baseline design, optimal from single-objective and Pareto members obtained by robust design method are 0.3, 0.4 and 0.5 respectively.
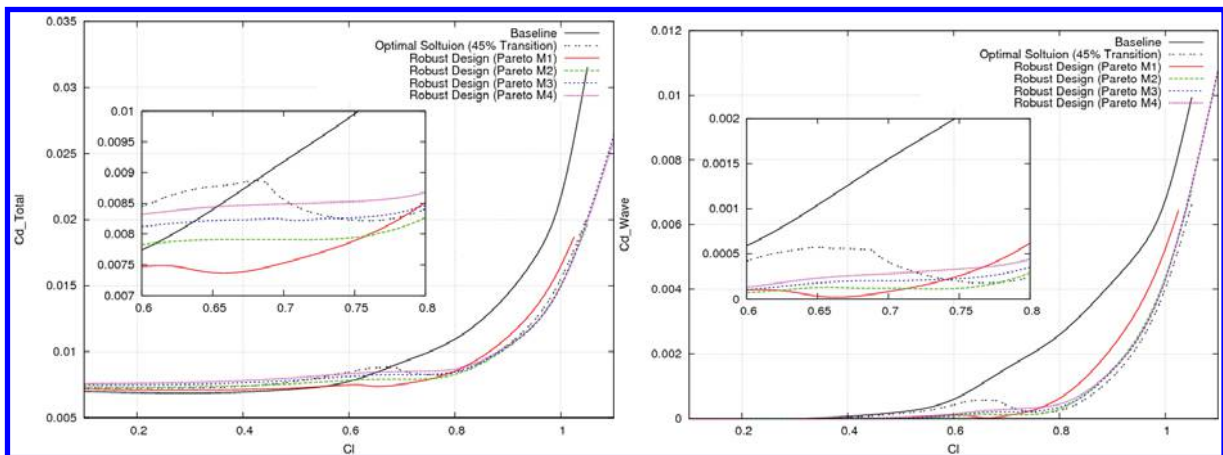
Figure 15. Cd_{Total} **(b) &** Cd_{Wave} **(c) vs.** Cl **at 25%c BLT.**

The baseline design with the optimal SCB obtained by the single-objective and robust design methods are also tested at six normal flight conditions shown in Table 8.

Table 8. Six flight conditions.

Conditions	M_∞	Re	Cl	x_{Trans} - $Upper$	x_{Trans} - $Lower$
Flight Condition 1	0.69	11.7×10^6	0.54	0.51	0.54
Flight Condition 2	0.69	11.7×10^6	0.69	0.51	0.54
Flight Condition 3	0.70	11.7×10^6	0.38	0.51	0.54
Flight Condition 4	0.70	11.7×10^6	0.50	0.51	0.54
Flight Condition 5	0.73	11.7×10^6	0.22	0.51	0.54
Flight Condition 6	0.73	11.7×10^6	0.34	0.51	0.54

The histogram shown in Figure 16 compares the total drag obtained by the baseline design, the single-objective (Section V.A) and the robust design approaches. It can be seen that the baseline design with the optimal SCB – robust Pareto member 1 produces lower total drag when compared to the baseline design and the optimal SCB obtained by the single-objective method. The optimal SCB - Pareto member 1 reduces the total mean drag by 36% while lowering the total drag sensitivity by 77%. The optimal SCB obtained in Section V.A reduces the total mean drag and sensitivity by 9.5% and 48% respectively even though it produces higher drag at the flight conditions 1, 3 and 5. Figure 17 compares the lift to drag ratio obtained by the baseline design, the optimal SCB from Section V.A and Pareto member 1. It can be seen that Pareto member 1 has a biggest lift to drag improvement at the flight condition 4.
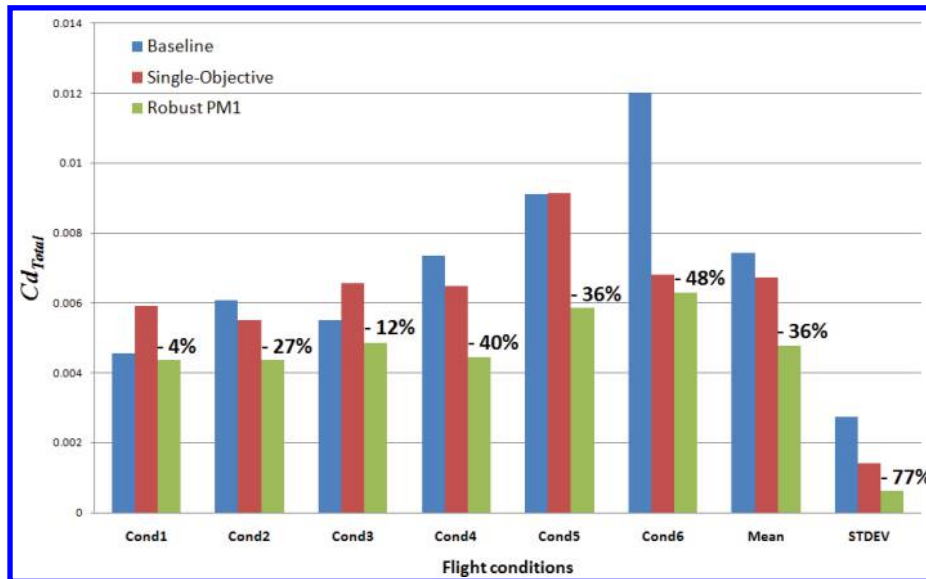
Figure 16. Drag reduction obtained by the baseline design, the single-objective solution and robust Pareto member 1 (Note: Robust PM1 represents Pareto member 1 obtained by the robust design optimisation. Mean and STDEV represent the mean and standard deviation of Cd_{Total} at six flight conditions).
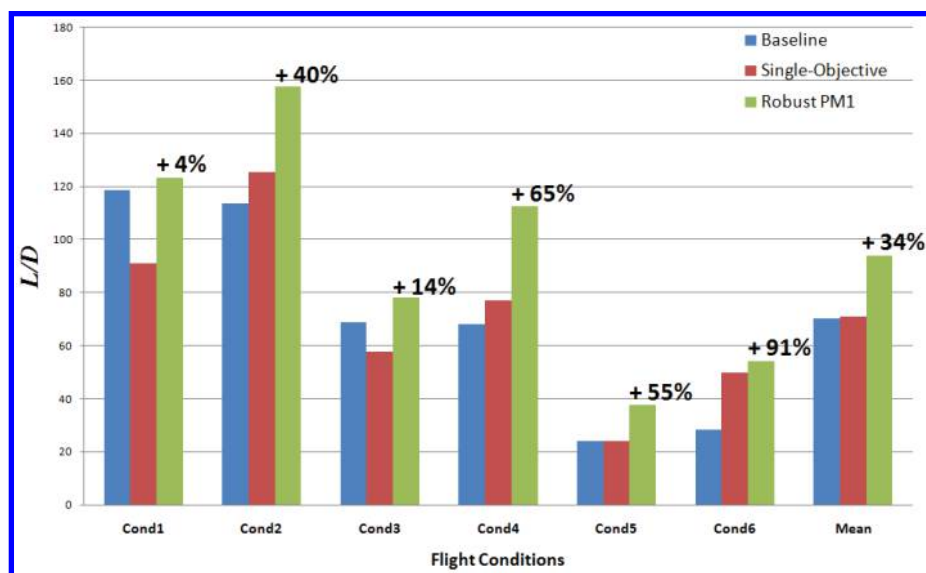
Figure 17. Drag reduction obtained by the baseline design, the single-objective solution and robust Pareto member 1.

16
American Institute of Aeronautics and Astronautics

One example (at the flight condition 4) is shown in Figure 18 where the pressure contours obtained by the baseline design and Pareto member 1 are illustrated. Even though the SCB obtained by Pareto member 1 is optimized at the critical flight condition, the optimal SCB – Pareto member 1 reduces the wave drag (Cd_{Wave} = 0.00250) obtained by the baseline design by 99.5% (Cd_{Wave} = 0.00001) and reduces the total drag by 40% which leads to 65% improvement of L/D when compared to the baseline design.
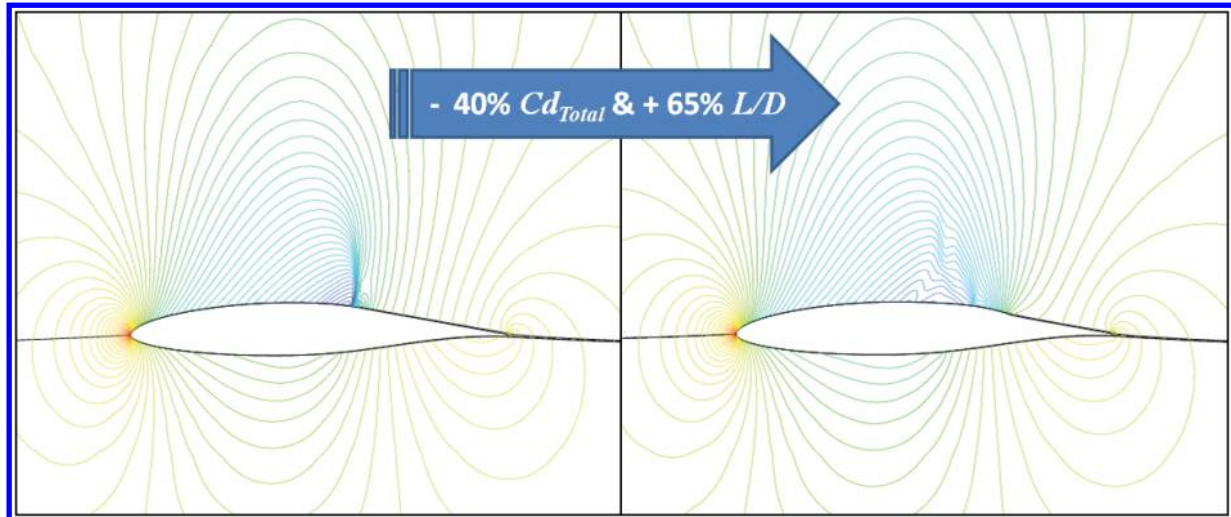
Figure 18. *Cp* contour comparison obtained by the baseline design (left) and Pareto member 1 (right).

To summarise the design test cases (Sections V.A and V.B), the design engineer can choose one of the solutions (Pareto members 1 to 4) obtained by robust multi-objective design optimisation due to two main reasons; the first is that even though the optimal solution from Section V.A produces lower total drag at the standard flight conditions (BLT position at 45%c), Pareto members 1 to 4 have lower sensitivity (stable: no fluctuation) at the variability of C_l and boundary layer transition positions [25%c:50%c]. In addition, it is clearly shown that applying SCB obtained by the robust design method stabilises the total drag of the baseline design at the both normal and critical flight conditions. The second is that Pareto members 1 to 4 have a smaller SCB than the optimal solution obtained by single-objective method. In other words, the manufacturer can save a material and weight cost and lower modification needed to the manufacturing system.

VI. Conclusion

In this paper, a robust evolutionary optimisation technique has been demonstrated and methodology for the design of adaptive wing/aerofoils that use Active Flow Control bump designs was developed. Analytical research shows the benefits of coupling optimisation method with robust design techniques to produce stable and high performance solutions. The use of SCB on an existing aerofoil can reduce significant transonic drag which will save operating and manufacturing cost as well as emission reduction. Future work will focus on robust design optimization of SCB on a 3D wing.

Acknowledgments

References

[1]Lee, D. S., Gonzalez, L. F., Srinivas, K., Periaux, J., Robust Evolutionary Algorithms for UAV/UCAV Aerodynamic and RCS Design Optimisation, *International Journal Computers and Fluids*. Vol 37. Issue 5, pages 547-564, ISSN 0045-7930. 2008.

[2]Lee, D. S., Gonzalez, L. F., Srinivas, K., Periaux, J., Robust Design Optimisation using Multi-Objective Evolutionary Algorithms, *International Journal Computers and Fluids*. Vol 37. Issue 5, pages 565-583, ISSN 0045-7930. 2008.

[3]Taguchi, G., Chowdhury, S., *Robust Engineering*, McGraw–Hill, New York, 2000.

[4]Lee, D. S., Gonzalez, L. F., Periaux, J., Srinivas, K., *Evolutionary Optimisation Methods with Uncertainty for Modern Multidisciplinary Design in Aeronautical Engineering*, Notes on Numerical Fluid Mechanics and Multidisciplinary Design (NNFM 100), 100 Volumes NNFM and 40 Years Numerical Fluid Mechanics. Pages 271-284, Ch. 3., Heidelberg: Springer-Berlin, ISBN 978-3-540-70804-9, 2009.

[5]Ashill, P. R., Fulker, L. J. and Shires, A., A novel technique for controlling shock strength of laminar-flow aerofoil sections. Proceedings 1st Europian Forum on Laminar Flow Technology, pp. 175-183, Hamburg, Germany, DGLR, AAAF, RAeS, March 16-18 1992.

[6]Qin, N., Zhu, Y. and Shaw, S. T., Numerical Study of Active Shock Control for Transonic aerodynamics, *International Journal of Numerical Methods for Heat & Fluid Flow*, Vol. 14 No. 4, pp 444 – 466, 2004.

[7]Wong, W.S., Qin, N., Sellars, N., Holden, H., Babinsky, H., A combined experimental and numerical study of flow structures over three-dimensional shock control bumps, *Aerospace Science and Technology*，Vol.12，pp436–447. 2008.

[8]Qin, N., Wong, W.S., LeMoigne, A., Three-dimensional contour bumps for transonic wing drag reduction, *Proc. IMechE, Part G: J. Aerospace Engineering*, Vol.222(G5), pp605-617. 2008.

[9]Lee, D. S., Gonzalez, L. F. and Whitney, E. J., *Multi-objective, Multidisciplinary Multi-fidelity Design tool: HAPMOEA – User Guide. The Univ. of Sydney*, Sydney, NSW, Australia. 2007.

[10]Hansen, N. and Ostermeier, A., Completely Derandomized Self-Adaptation in Evolution Strategies. Evolutionary Computation, 9(2), pp. 159-195, 2001.

[11]Koza, J., *Genetic Programming II*. Massachusetts Institute of Technology, 1994.

[12]Michalewicz, Z., *Genetic Algorithms + Data Structures = Evolution Programs*. Artificial Intelligence, Springer-Verlag, 1992.

[13]Wakunda, J., Zell, A., Median-selection for parallel steady-state evolution strategies. In Marc Schoenauer, Kalyanmoy Deb, Günter Rudolph, Xin Yao, Evelyne Lutton, Juan Julian Merelo, and Hans-Paul Schwefel, editors, ParallelProblem Solving from Nature – PPSN VI, pages 405–414, Berlin, Springer, 2000.

[14]Van Veldhuizen, D. A., Zydallis, J. B., Lamont, G. B., Considerations in Engineering Parallel Multiobjective Evolutionary Algorithms, *IEEE Transactions on Evolutionary Computation*, Vol. 7, No. 2, pp. 144-17, 2003.

[15]Sefrioui, M., Périaux, J., A Hierachical Genetic Algorithm Using Multiple Models for Optimization. In M. Schoenauer, K. Deb, G. Rudolph, X. Yao, E. Lutton, J.J. Merelo and H.-P. Schwefel, editors, Parallel Problem Solving from Nature, PPSN VI, pages 879-888, Springer, 2000.

[16]Deb, K., Multi-objective genetic algorithms: Problem difficulties and construction of test problems. *Evolutionary Computation Journal*, 7(3), pages 205-230, 1999.

[17]Drela, M., *A User's Guide to MSES 2.95*. MIT Computational Aerospace Sciences Laboratory, September 1996.

[18]Lee, D. S., Periaux, J., Pons-Prats, J., Bugeda, G. and Onate, E., Double Shock Control Bump Design Optimisation Using Hybridised Evolutionary Algorithms. Special Session (S035 – IEEE CEC): Evolutionary Computation in Aerospace Sciences, 2010 IEEE World Congress On Computational Intelligence (WCCI 2010), Barcelona Spain, July 18-23rd 2010.

[19]Iman, R. L., Davenport, J. M., Zigler, D. K., *Latin Hypercube Sampling (Program User's Guide)*, OSTI 5571631 1980.